Pak. J. Bot., 58(2): 605-614, February 2026.

ARTICLE | DOI: http://dx.doi.org/10.30848/PJB2026-2(14)

FORMULATION AND CHARACTERIZATION OF NOVEL *BACILLUS SUBTILIS* LOADED STARCH NANOPARTICLES AGAINST FUNGAL PATHOGENS

AYESHA KHAN AND SADIA JAVED*

Department of Biochemistry, Government College University, Faisalabad, Pakistan

*Corresponding author's email: sadiajaved@gcuf.edu.pk

Abstract

The aim of the current study was to synthesize and characterize the *Bacillus subtilis*-loaded starch nanoparticles against fungal pathogens. The starch nanobeads were synthesized via ultra-sonication and *Bacillus subtilis* was subsequently encapsulated onto the beads. The *Bacillus subtilis* loaded starch nanoparticles were characterized by XRD and SEM to confirm the crystalline structure and spherical shape of nanobeads. *Bacillus subtilis* loaded starch nanoparticles showed a Z-average size of 245 nm and zeta potential of −20.25 (mV) as indicated by zeta potentials. FTIR analysis demonstrated the interactions between starch nanobeads and *Bacillus subtilus*. The antifungal potential was tested against *Fusarium oxysporum, Fusarium graminearum, Aspergillus flavus, Alternaria solani, Botrytis cinerea, Verticllium dahlia,* and *Cladosporium cucumirinum*. A clear inhibition zone and minimum inhibition concentration (MIC) was observed that indicates the significant antifungal effect of the *Bacillus subtilis* loaded starch nanoparticles. Functional effectiveness of *Bacillus subtilis* starch nanoparticles for practical uses could be among the primary concerns of future research.

Key words: Nanoparticles; Biopolymer; Pathogen; Encapsulation; Fungicide; Biocontrol

Introduction

Enhancing agricultural productivity to meet the increasing demands for food and ensuring food security are crucial tasks in addressing the growing population. Protecting human food resources and agricultural yields heavily relies on the effective management of diseases (Murhekar *et al*., 2021). One of the primary challenges encountered in agriculture is the infestations and diseases caused by fungi, bacteria, pests, and various pathogens. Among agricultural settings, phytopathogenic fungi are responsible for various diseases compared to other environmental pathogens. Fungi can colonize various substrates and to adapt any medium even in harsh environments. They can impact crops at any stage, from sowing to postharvest, utilizing chemical products that are cost-effective and easily accessible to manage phytopathogenic fungi. The indiscriminate use of chemical agents gives rise to several problems such as ecological disturbances, and diseases in animals and humans. According to (Santoso *et al.*, 2022), chemical products that are inexpensive and readily available are employed to control phytopathogenic fungi. In addition, fungi have demonstrated enhanced resistance and potency against chemical agents. Nowadays, effective and eco-friendly substitutes such as plant extracts, essential oils, and biological control agents are being used to combat phytopathogenic fungi. These substitutions are considered highly advantageous due to their positive outcomes. However, despite their benefits, these alternatives encounter challenges such as delayed effects, high costs of acquisition, and the need for frequent applications, rendering them susceptible (Cruz-Luna *et al*., 2021).

Microbes create metabolites that are known to improve plant development, carry out effective biocontrol operations, guarantee large-scale production, maintain appropriate structure, and be readily accessible (Elnahal *et al*., 2022). Plant diseases caused by microorganisms lead to significant losses in crops (Shahzad *at el*., 2021). The utilization of biological control methods diminishes the harm caused by pathogenic attacks, without posing hazards to the environment (Barton *et al*., 2020). The utilization of *Bacillus* spp., (Javed *at el*., 2024). as a biological control agent is widely acknowledged for its ability to generate potent antifungal compounds targeting various phytopathogenic fungi (Santoso *et al*., 2021). *Bacillus subtilis* is a Gram-positive bacterium renowned for its economic and effective entomopathogenic properties, serving as efficient biopesticides. The pesticidal activity of *Bacillus subtilis* is due to the synthesis of insecticidal proteins. The majority of these proteins are synthesized and encapsulated during sporulation, leading to parasporal crystal formation, distinguishing *Bacillus subtilis* from other *Bacillus* spp., (Gul *at el*., 2023). Formulations combining *Bacillus subtilis* spores and parasporal crystals are considered safer and more precise alternatives to synthetic pesticides, constituting a significant portion of microbial-based biopesticides in the market. *Bacillus subtilis* produces crystal proteins (Cry) that are toxic to various insects, underscoring its role as a microbial pesticide and insecticide for enhancing plant resistance through genetic modification (Jurat-Fuentes *et al.*, 2021). Encapsulation is the act of enclosing active components like cells, tissues, and microbes within a protective shell. This method ensures the genetic reliability of products and provides support in various environmental conditions, thus preserving active ingredients for extended

Received: 03-02-2025 | Revised: 25-08-2025 | Accepted: 30-08-2025 | Online: 24-10-2025

periods. Microbial agents are susceptible to factors that can reduce their effectiveness and reliability, such as exposure to UV radiation and unfavorable temperatures (John *et al*., 2011). Encapsulation presents a solution to overcome these challenges, especially in agriculture. It brings benefits like reducing losses, enhancing ecological stability, improving efficiency, and increasing commercial viability. Utilizing bioactive compounds in the formation of biofertilizers, bioinsecticides, and other products is a promising approach (Brindha *et al*., 2024). Different polymers are used as protective walls in encapsulation, such as Chitosan gums, starch, pectin, and others. These polymers help retain desired compounds in the system and extend the release of bioactive compounds (Alhaithloul *et al*., 2024).

In this work, the potential of *Bacillus subtilis* as a sustainable alternative to synthetic agrochemicals for disease management in agriculture was observed. The primary objective of this work was to validate the efficacy of *Bacillus subtilis* and to evaluate the benefits of encapsulation technology in enhancing stability, targeted delivery, and control release. By focusing on the unique properties of *Bacillus subtilis* and the benefits of encapsulation, the purpose of this work was to develop eco-friendly and sustainable agricultural practices. To assess the *Bacillus subtilis*-loaded starch nanobeads potential as efficient carriers, the study aims to offer a comprehensive characterization of them, focusing on important elements including surface charge, morphology, size, and structural veracity. The study we conducted integrates several characterization methods, such as XRD, FTIR, and SEM, Microbial cells are encapsulated to improve their vitality and stability against fungal infections. X-RD, Fourier Transform Infrared Spectroscopy, and scanning electron microscopy are used to characterize capsules and analysis of its antifungal properties.

Materials and Methods

Preparation of starch nanoparticles

Material preparation: Rafhan Maize Products (Faisalabad), which is associated with global corporations and ensures high-quality products, provided maize starch with a weight percentage composition of 73 ± 1 amylopectin and 27 ± 1 amylose. Sigma-Aldrich (Darmstadt, Germany) supplied the sodium hydroxide (ACS reagent ≥ 97%, molecular weight: 40), calcium chloride (molecular weight: 110.98 g/mol), and sodium alginate (viscosity, 5 – 40 cps, gluconate monomer units ≥ 60%). We acquired the Bacillus subtilis freeze-dried culture and more materials from the Industrial Biotechnology Lab of the Department of Biochemistry at Government College University in Faisalabad (GCUF) (Azeem *at el.*, 2022; Bashir *at el*., 2022).

Activation of *Bacillus subtilis* culture: To prepare a culture plate of bacterial strain, 100ml of the distilled water was added to 500ml beaker along with 0.8g nutrient broth and 4g Agar and the beaker was covered with aluminum foil. Then sterilized in an autoclave at 80ºC along with Petri plates (Azeem *at el*., 2022). After autoclaving, all subsequent steps were performed in a sanitized Laminar Air Flow. The sterilized Petri plates were filled with the prepared medium and allowed to solidify for a few minutes. A liquid culture of the bacterial strain was streaked onto the plates using a red-hot sterilized rod. The plates were then sealed with parafilm and incubated for 24 hours to allow bacterial growth (Bashir *at el.*, 2022).

Preparation of starch nanoparticles

Synthesis of nano-capsules or beads via ultra-sonication: Starch-based nano-capsules were synthesized using a modified version of the method described by Ahmad *et al*. A 10% (w/v) starch solution was prepared by dissolving 25.00 g of maize starch in 250 mL of distilled water. The mixture was then agitated in an incubator shaker (WIS-20, Germany) at 60°C for 30 minutes. This solution was subjected to ultrasonication using a sonicator (VCX750, Sonics & Materials, Inc., Newtown, CT, USA) operating at a power of 750 W and a frequency of 50 kHz. To prevent overheating, ultrasonication was performed for 30 minutes in 5-minute intervals. Ultrasonication generates intense shear forces that can disrupt the structure of starch granules, breaking them into smaller particles and modifying their physicochemical properties. This reduction in particle size is critical for the formation of starch-based nano-capsules or beads and for achieving nanoscale dimensions. Additionally, ultrasonication promotes uniform dispersion of starch molecules, preventing aggregation and ensuring the production of homogeneous and stable nano-capsules. After sonication, the starch suspension was stored at 4°C for 24 hours. High-intensity ultrasonication is widely used in processes such as emulsification, dispersion, and particle size reduction (Shoukat *at el*., 2024). Notably, ultrasonication has minimal impact on the polymorphic structure of starch (Sandhya *et al.,* 2021). Although significant changes in X-ray diffraction patterns and crystallinity are not typically observed, a decrease in the enthalpy of gelatinized maize starch has been reported. This is attributed to the partial breakdown of the starch's double-helical structure. A reduction in viscosity of gelatinized starch solutions following ultrasonication has also been documented (Hassainia *et al*., 2018).

Centrifugation and lyophilization: The refrigerated starch suspension was transferred into 15 mL Falcon tubes and centrifuged at 350 rpm. Centrifugation is a widely used technique in various disciplines such as pharmacy, biochemistry, and medicine to separate components within a mixture. It operates by applying a centrifugal force that enables the separation of substances based on their size, shape, or density. Samples that do not settle under standard conditions may be subjected to increased centrifugal force to accelerate sedimentation. This process plays a crucial role in the isolation of biomolecules from complex mixtures (Olatunde, 2024). Following centrifugation, the supernatant was removed, and the pellet was subjected to lyophilization (freeze-drying). In this process, the sample was initially frozen, after which the surrounding pressure was reduced to enable the sublimation of water directly from the solid (ice) to the gaseous phase. This technique ensures the removal of moisture while preserving the structural and functional integrity of the sample. One of the main challenges in solvent extraction and drying is to retain the physicochemical properties of the original material while maximizing product recovery (Shoukat *at el*., 2024; Paredes *et al*., 2016). After lyophilization, the dried starch

was transferred to sterile Petri plates and left at room temperature for an additional 24 hours to ensure complete drying. The resulting solid was then ground into a fine powder using a sterile mortar and pestle. This powdered form facilitates further characterization and application.

Encapsulation of *Bacillus subtilis* in starch beads or capsules: A 2% (w/v) starch solution was prepared using lyophilized starch powder. To begin, 100 mL of distilled water was added to a beaker and heated on a hot plate. The beaker was covered with aluminum foil to maintain sterility, and a thermometer was inserted through a small opening to monitor the temperature. The temperature was maintained at 75°C and carefully monitored to ensure it did not exceed 80°C, as starch begins to lose its functional properties beyond this threshold. Once the solution reached 75°C, the hot plate was turned off, and 2 g of lyophilized starch powder was gradually added to the heated water in small raises with continuous stirring using a magnetic stirrer to prevent lump formation. After the starch had fully dissolved, 5 µL of nutrient broth containing *Bacillus subtilis* was added to the solution to initiate encapsulation within the starch matrix (Shoukat *at el*., 2024) The solution was maintained at a pourable consistency to ensure proper bead formation. To enhance bead stability and provide binding capacity, 2 g of sodium alginate was added to the mixture and stirred continuously until fully dissolved. Separately, a 3% (w/v) calcium chloride ($CaCl_2$) solution was prepared and poured into a sterile Petri plate. Using a sterile pipette, the starch-alginate *Bacillus subtilis* mixture was dropped into the $CaCl_2$ solution, allowing bead formation via ionic gelation. The Petri plate was then placed in a freezer at −20°C for 24 hours to solidify the beads. After incubation, the beads were carefully collected from the $CaCl_2$ solution and soaked in fresh nutrient broth containing *Bacillus subtilis* for 1 hour under gentle shaking to promote bacterial enrichment. Following this, the nutrient broth was discarded, and the beads were harvested and stored in sterile Eppendorf tubes. For antifungal activity assessment, the beads were dissolved in dimethyl sulfoxide (DMSO) and tested as described by (Akalin & Pulat, 2020).

Characterization of sonicated nanoparticles: The morphological characteristics of the ultrasonically produced starch nanoparticles were described. Using a scanning electron microscope (Emcraft cube series, Korea) at the Department of Physics (Government College University, Faisalabad), electron micrographs of the starch nanoparticles' surface morphology were examined. SEM was performed in a low vacuum field maintained at 8 kV with a working distance of 12.33 mm. Every scan was carried out three times. With certain modifications, the analysis was carried out using Atraki and Azizkhani's methods (Atraki & Azizkhani, 2021).

Encapsulation efficiency: With some slight modifications, the method of (Afzaal *et al*., 2020*)*. was used to evaluate the *Bacillus subtilis*-loaded microbeads' encapsulation efficiency (EE%). A stomacher was used to separate the encapsulated *Bacillus subtilis* from the phosphate buffer solution (Seward, UK). After centrifuging the resulting solution, an Eppendorf Bio Spectrometer® basic (Germany) was used to determine the absorbance of the supernatant spectrophotometrically at 306 nm. The following formula was used to calculate the EE percentage:

$$EE\% \text{ is } (N/No) \times 100$$

$$EE\% \text{ is } (N/No) \times 100 \qquad (1)$$

Here, N is the number of remaining embedded cells that were eliminated, and No is the starting number of free cells that were added.

Size of particles and zeta potential: The electrical potential difference between nanoparticles and their surrounding medium was measured using zeta potential. The particle size and zeta potential of *Bacillus subtilis*-loaded microbeads were determined using Ahmad and Gani's methodology (Ahmad & Gani 2021). To completely disperse the particles, 0.02% (w/v) of the sample was sonicated in Milli-Q water at 40 kHz for a few minutes in a sonication bath before measurement. The cuvette was then filled with a 3 ml sample, and a zeta sizer was used to take the measurement. Before measurement, For the whole night, these 0.02% (w/v) samples were left to settle in KCl (0.10 mM) at a pH approximately neutral. The units used to measure size, and zeta potential were nm and mV, respectively. To determine the mean value, the measurement was made three times.

Scanning electron microscopy (SEM): The dried powder that is obtained after lyophilization was subjected to scanning electron microscopy (SEM) to analyze the morphology, particle size and crystallinity of the starch particles. In this method, an electron beam originating from a particular source such as tungsten strikes on the surface of the specimen for visualization. The electrons are affected by the electromagnetic field produced by lenses, compelling the electron beam to interact with the surface of the specimen. Consequently, the electrons undergo diffraction in various orientations and produce multiple signals that are capable of being visualized on a display or screen. The average size determined through Scanning Electron Microscopy (SEM) is similar to the outcomes achieved through dynamic light scattering (Paredes *et al*., 2016). The samples were then automatically analyzed using computer software.

X-ray diffraction: The XRD analysis was executed on powders of pure wall materials. The crystallinity and particle size were analyzed using an X-ray diffractometer (XRD). Diffraction arises from the scattering of light by a periodic array characterized by long order, leading to the occurrence of constructive interference at specific angular orientations. The atoms constituting a crystalline structure are positioned in a repeating pattern, hence enabling the phenomenon of light diffraction. X-ray wavelengths permit resemblance to the interatomic distances, a feature utilized in X-ray Diffraction methodologies to find crystalline properties of various materials. The interaction of X-rays with atoms results in the generation of a diffraction pattern that encodes details about the atomic configuration within the crystal

lattice. In contrast, amorphous substances such as glass lack the presence of a periodic array with long-range order, thereby precluding the emergence of prominent peaks in the diffraction pattern (Chauhan & Chauhan, 2014).

FTIR analysis: Fourier-transform infrared (FTIR) spectroscopy was conducted to confirm the encapsulation of *Bacillus subtilis* into starch beads. For the identification of functional of characteristic functional groups present in both the maize starch matrix and the bacterial components. To assess the structural integrity of the starch beads after encapsulation, the dried samples were ground with KBr pellets and pressed into a mold. The infrared spectra were measured in the wavelength range of 4000–5000 cm-1 at a resolution of 4 cm-1 using a Perkin Elmer FTIR spectrophotometer. Antifungal activities of the produced fungicides were screened by using the agar well diffusion method. One ml of spore (adjusted to 106 spores' ml-1) of freshly prepared fungal pathogens was inoculated into each plate containing 25 ml of agar medium. Freeze-dried fungicides were dispersed by ultra-sonication in deionized water. Samples were withdrawn to elucidate the effect of antifungal compounds on fungal growth (McMullan *et al.,* 2023).

Antifungal activity: Antifungal activity of starch capsules or beads against *Fusarium oxysporum*, *Aspergillus flavus, Aspergillus niger, Alternaria solani*, *Botrytis cinerea,* and *Verticillium dahliae* was performed with the same well diffusion method. In antifungal activity, only two wells were made one is loaded with samples other one is blank. The nutrient media used in antifungal activity is potato dextrose agar media (PDA) media. PDA media was collected from the Plant Microbe Integration Lab, Department of Botany, Government College University Faisalabad. Plates were placed in an incubator at 37°C temperatures for 72 hours. After 72 hours inhibition zones (around the well where there is no growth of fungi and bacteria) were measured with the help of scale. By evaluating the antibacterial and antifungal activities, it is ensured that the bacteria remain viable and effective against targeted pathogens after encapsulation. These activities were assessed to verify that the encapsulation process has not adversely affected the bacterial efficacy and prove that the starch beads or capsules provide a suitable environment for sustained bacterial activity (Kleindorfer *et al*., 2021).

Results and Discussion

Characterization of sonicated nanoparticles: Scanning Electron Microscopy (SEM), a powerful analytical technique capable of producing high-resolution, high-magnification images, was employed to examine the morphological characteristics of the sonicated starch nanoparticles. The resulting micrographs are presented in Fig. 1. The morphology of the nanoparticles exhibited features characteristic of nano-beads synthesized via ultrasonication, as reported in recent studies. The SEM images revealed that the starch nano-beads had relatively smooth surfaces and predominantly round or oval shapes. These observations are consistent with the findings of (Ashwar *et al*., 2014), who reported that rice starch nanoparticles exhibited spherical shapes with uniform surface patterns. Similarly, in the current study, some starch nanoparticles displayed regular geometric features, although variations such as oval or slightly irregular forms were also observed. These morphological inconsistencies may be attributed to the ultrasonication process, which can cause deformation of starch granules, leading to the formation of aggregates or tracheid-like structures. As reported by Ahmed, (Ahmad *et al.,* 2019), the presence of small, dispersed granules within the nanoparticle matrix is a common feature of sonicated starch. Furthermore, the high density of hydroxyl groups on the starch surface promotes intermolecular interactions, contributing to nanoparticle agglomeration (Nichols *et al*., 2022). This tendency toward aggregation results in variability in particle size and shape, which can complicate accurate morphological analysis by SEM and lead to a lack of consistent patterning (Robson *et al*., 2022). (Dong *et al*., 2022) noted similar issues in their nanoprecipitation-based study of four starch types, which also produced unstable colloidal dispersions prone to aggregation. These findings highlight the inherent instability of starch nanoparticles and the challenges associated with maintaining uniform morphology.

Encapsulation efficiency: Sonicated starch nanoparticles were utilized to synthesize microbeads encapsulating *Bacillus subtilis*. The encapsulation efficiency was calculated using Equation (1), as described earlier. After encapsulation, the viable cell counts of *Bacillus subtilis* decreased from an initial value of 10.62 log CFU/mL to 9.05 log CFU/mL. A statistical analysis yielded a p-value of 0.03, indicating that the observed difference in mean values was statistically significant. Table 1 presents the calculated encapsulation efficiency and highlights its influence on the viability of *Bacillus subtilis* during the final stage of encapsulation. The inclusion of sodium alginate alongside starch provided enhanced mechanical strength and facilitated effective crosslinking, thereby improving the encapsulation of *Bacillus subtilis*. In a previous study, *Bacillus subtilis* encapsulated in horse chestnut starch nanoparticles exhibited an encapsulation efficiency of 89.11% (Klionsky *et al*., 2021). The results of the present study, which involved encapsulating *Bacillus subtilis* isolated from camel milk in starch-based nanobeads, showed a comparable encapsulation efficiency of 78.00%. These findings align with previous research, demonstrating the effectiveness of starch-based nanoparticles in probiotic delivery systems.

Table 1. Particle size, Zeta potential, and Encapsulation efficiency of starch nanoparticles with and without *Bacillus subtilis*.

No of treatments	Particle size	Zeta potential	Encapsulation efficiency (%)
Starch Nano particles without bacteria	4.62 ± 2.02	−18.32 ± 4.10	–
Starch Nano particles with bacteria	5.89 ± 2.03	−20.25 ± 2.02	78.00 ± 4.00

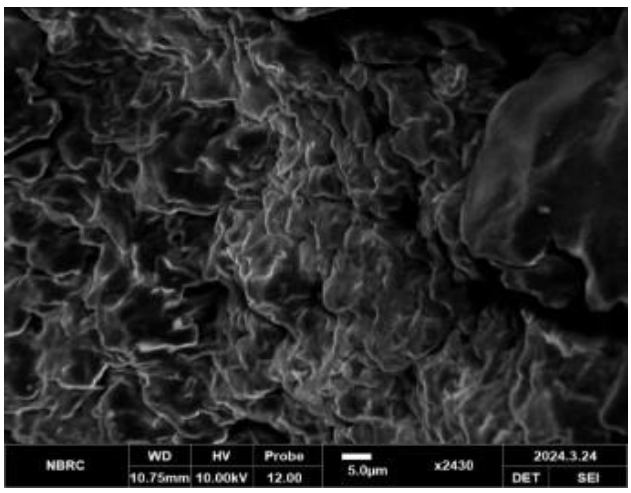

Fig. 1. SEM-based morphological representation of starch nanoparticles.

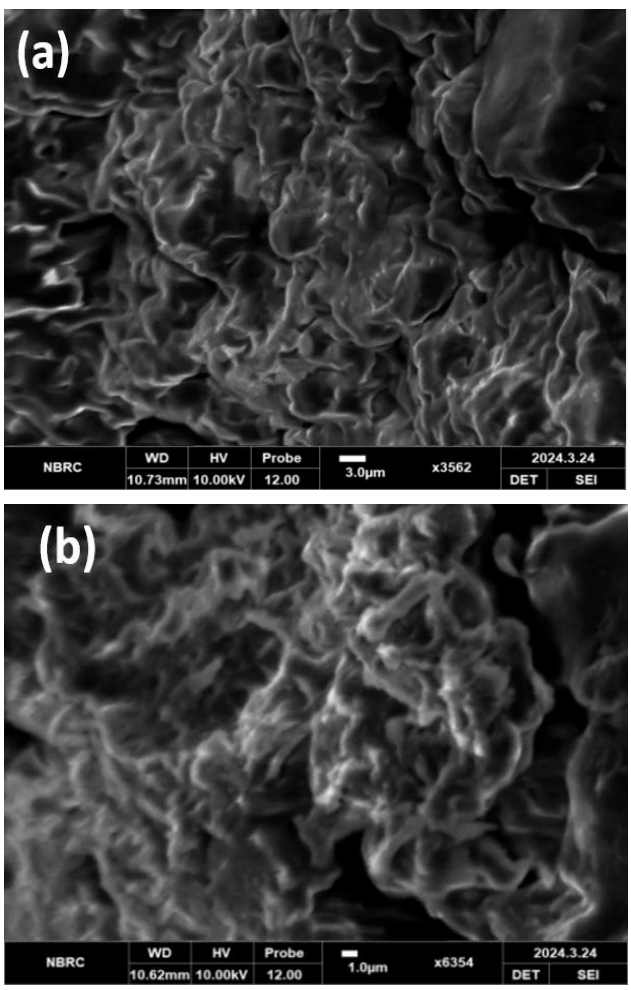

Fig. 2. Characterization with scanning electron microscopy a) and b) At the magnification of 3um and 1um.

Zeta size and potential: The particle size of polymer-based nanoparticles plays a crucial role in determining structure–activity interactions and must be accurately monitored to avoid errors arising from incomplete substrate dissolution, size correction artifacts, or aggregation during shearing and separation (Le Quéré *et al*., 2016). Table 1 summarizes the average particle sizes of the microbeads with and without *Bacillus subtilis* encapsulation. The average particle diameter was 5.82 µm for *Bacillus subtilis*-loaded microbeads and 4.62 µm for those without the probiotic. The increase in size upon encapsulation suggests the successful incorporation of *Bacillus subtilis* within the starch nanoparticle matrix. This result is consistent with previous findings demonstrating that an increase in particle size is indicative of effective microbial encapsulation (Atraki & Azizkhani, 2021). Xiao *et al*., reported that rice starch nanoparticles exhibited sizes around 200 nm, significantly smaller than those produced in the current study. This discrepancy can be attributed to differences in starch origin and processing method. The ultrasonication treatment used in this study effectively broke down the amylopectin structure, contributing to the observed reduction in base particle size prior to encapsulation (Sun *et al*., 2009) encapsulated *Bacillus subtilis* using a pectin–alginate matrix and observed microbead sizes around 5.89 µm, which is comparable to the sizes obtained in this study. Similarly, (Zubair & Bandyopadhyay, 2023) reported that taro starch microbeads exhibited diameters of 4.62 µm without *Bacillus subtilis* and 5.82 µm with encapsulation—values that align closely with our findings. Regarding surface charge, zeta potential measurements indicated a significant difference between the two formulations. As shown in Table 1, the zeta potential of *Bacillus subtilis*-loaded microbeads was −20.25 mV, whereas that of unloaded microbeads was −18.32 mV. A higher negative zeta potential enhances electrostatic repulsion and reduces Van der Waals interactions between particles, contributing to colloidal stability (Masoudipour *et al.,* 2017). The increased surface charge in the loaded beads is likely due to the surface properties of *Bacillus subtilis*, which interact with the starch matrix and alter surface chemistry. Although a zeta potential greater than ±25 mV is generally considered optimal for nanoparticle stability, encapsulation matrices such as starch and sodium alginate can provide additional physical barriers that prevent aggregation, even at slightly lower zeta potential values. Ahmad *et al*., reported that water chestnut starch nanoparticles loaded with *Bacillus subtilis* had a zeta potential of −20.00 mV, closely matching the value observed in this study. The negative surface charge prevents recombination of particles, thereby enhancing nanoparticle dispersion and long-term stability. Overall, the observed changes in particle size and zeta potential confirm the successful encapsulation of *Bacillus subtilis* within starch-based Nano carriers. The slightly reduced zeta potential in the presence of the probiotic reflects surface modifications due to bacterial integration. Notably, the method used in this study produced microbeads with a more negative surface charge than those formed using nanofiber electrospun carriers (Atraki & Azizkhani, 2021), suggesting that ultrasonication-assisted encapsulation may offer superior colloidal stability.

Scanning electron microscopy (SEM): Scanning Electron Microscopy (SEM), a high-resolution imaging technique widely used to investigate surface morphology, was employed to examine the structural characteristics of microbeads. The SEM images are presented in Fig. 1. Starch nanoparticles without *Bacillus subtilis* exhibited smooth cubic and tubular structures. As shown in Fig. 2, micrographs of beads with and without *Bacillus subtilis* did not display any visually distinct differences in surface morphology. This observation aligns with the findings of (Yadav *et al*., 2022), who also reported no visible presence of *Bacillus subtilis* on the surface of the

encapsulation matrices in SEM images. This is likely due to the limitations of SEM, which only reveals surface features and cannot detect bacteria embedded within the matrix (Martin *et al*., 2023). Despite the overall smooth morphology, some regions of the micrographs showed granular structures with void spaces between them, suggesting a gel-like network. The *Bacillus subtilis*-loaded microbeads exhibited predominantly oval or round shapes with smooth and porous surfaces. Some particles displayed polygonal grains with smooth edges on one side and ridges or surface irregularities on the other. The SEM analysis of starch nanoparticles encapsulating *Bacillus subtilis* revealed symmetrical structures and circular forms, consistent with the findings of (Atraki & Azizkhani, 2021), who described probiotic-loaded starch granules as smooth and spherical in appearance. Similarly, (Noman *et al*., 2023) characterized *Bacillus subtilis* encapsulated in starch-based matrices as having round, uniform surfaces. Ahmad *et al*., (2019) reported that encapsulated probiotics within starch nanoparticles appear as granular or oval forms. However, in the present study, the encapsulated *Bacillus subtilis* was not clearly visible in the SEM images, likely due to its entrapment within the internal matrix. This is consistent with earlier work by (Fareez *et al*., 2015), who demonstrated that *Bacillus subtilis* encapsulated in alginate-xanthan beads was not visible on the surface, indicating successful internal entrapment. Overall, the SEM results confirmed the formation of well-structured microbeads with smooth surfaces and consistent morphology. The internal encapsulation of *Bacillus subtilis* was supported by the absence of bacterial structures on the outer surface, highlighting the efficiency of the encapsulation method.

FTIR analysis: Fourier Transform Infrared (FTIR) spectroscopy was employed to investigate the interactions between *Bacillus subtilis* and starch nanobeads produced through sonication. The FTIR technique provides valuable information about the absorption and transmission of infrared light by materials, allowing the identification of both inorganic and organic components. This is achieved through the characteristic absorption frequencies of different molecular groups, typically ranging from 600 to 4000 cm^{-1}. FTIR spectra of the *Bacillus subtilis*-loaded starch nanobeads revealed prominent peaks at 3221.58 cm^{-1} and 2946.47 cm^{-1}, corresponding to the stretching vibrations of the O–H group in carboxylic acids. A peak at 2168.94 cm^{-1} was attributed to the C–N stretching of amine groups. Additionally, the amide group (N–H) was represented by peaks at 1606.38 cm^{-1} and 1422.90 cm^{-1}. Other significant peaks included 1352.84 cm^{-1} (phenolic O–H stretch), 1181.73 cm^{-1} (C–O stretching in aliphatic ethers), 1022.49 cm^{-1} (C–O stretching in alcohols), and 825.99 cm^{-1} (C–H wagging vibration). For the starch nanoparticles without *Bacillus subtilis*, FTIR spectra displayed peaks at 3217.74 cm^{-1} and 2945.44 cm^{-1}, corresponding to carboxylic acid (O–H) groups. A distinct peak at 2006.53 cm^{-1} was observed for C=C conjugation, and additional peaks at 826.07 cm^{-1} and 592.94 cm^{-1} were assigned to halo compounds (Fig. 3). The FTIR spectrum of the *Bacillus subtilis*-encapsulated nanobeads indicates the presence of various functional groups, suggesting the involvement of carboxylic acids, esters, fatty acids, triterpenoids, amines, amides, and other secondary metabolites from the encapsulated bacteria. Furthermore, the spectra provide insights into the capping and reduction effects of bacterial extracts on the nanoparticles, as evidenced by the functional groups present.

XRD analysis: In order to analyze the properties of microcapsules made from nanoparticles, crystallinity is an important consideration. Crystalline parts may act as a barrier to shield *Bacillus subtilis* from damaging environmental variables such as moisture, heat, and enzyme degradation (Le Quéré *et al*., 2016). *Bacillus subtilis* must have a controlled release; a higher crystallinity results in slow rate of breakdown for a more tenacious release. Early *Bacillus subtilis* release may result from amorphous regions' increased susceptibility to water absorption and rapid rate of breakdown. Consequently, there must be a balance between crystalline and amorphous components for nano and microscale capsule optimization (Feng *et al*., 2021). XRD can be used to describe nanoparticles of any size, as shown in Fig. 4, which shows changes in the locations of the diffraction peaks. Depending on the size and shape of the nanoparticle, conclusions can be made about the cellular characteristic factors and the crystal sections with an amorphous structure. XRD can also be used to investigate the creation of crystal structures as well as their chemical and physical characteristics. XRD analysis was performed to determine the crystallinity exerted from the structure of *Bacillus subtilis*-loaded microbeads in starch nanoparticles. The *Bacillus subtilis*-loaded microbeads' crystallinity points were shown by sharp peaks. Peak dispersion underneath amorphous humps also showed that certain areas had lost their crystallinity. The starch nanoparticle arrangements have been shown by the strong crystallinity peaks. The physical appearance of the amorphous structure matched the *Bacillus subtilis* incorporation. The combination of crystalline and amorphous regions caused the peaks to seem disorganized (Hassainia *et al*., 2018).

The findings of this study indicated that the size of sonicated starch nanoparticles in *Bacillus subtilis*-loaded microbeads influenced their transmissibility. The process of ultrasonication used for the production of starch nanoparticles, along with the encapsulation technique employed to create the microbead structures, altered the natural starch structure by breaking down the starch crystals in the granules. The FTIR spectrum of the starch nanoparticles showed characteristic peaks that reflected changes in the O–H and C–H bonds due to the encapsulation of *Bacillus subtilis*, resulting in an expanded vibration in comparison to the free *Bacillus subtilis* cells. Moreover, the presence of lipids and *Pediococcus acidolactici* was indicated by an influential band at 1748 cm^{-1}, which was attributed to C–O vibrations (Ahmad *et al*., 2019). Additionally, the starch nanoparticles, derived from rice and water chestnut, displayed structural characteristics such as hydrogen bonding and electrostatic forces. The highest absorption peak was observed at 3289 cm^{-1}, corresponding to the O–H stretch, which is consistent with previous findings by (Noman *et al.,* 2023). The current study's results were in agreement with earlier research by (Remanan & Zhu, 2021) and (Shahzad *et al*., 2021), as evidenced by absorption bands at 997 cm^{-1}, associated with the stretching of C–O–H, C–O, and C–O–C bonds, which are characteristic of encapsulated rutin in maize starch nanoparticles. The formation of hydrogen bonds between amide and carboxyl groups, indicated by the broadening of O–H stretching peaks between 3200 and 3700 cm^{-1}, was also observed, consistent with findings from a study on *Bacillus subtilis* encapsulation using zein and pectin (Gopalakrishnan *et al*., 2018).

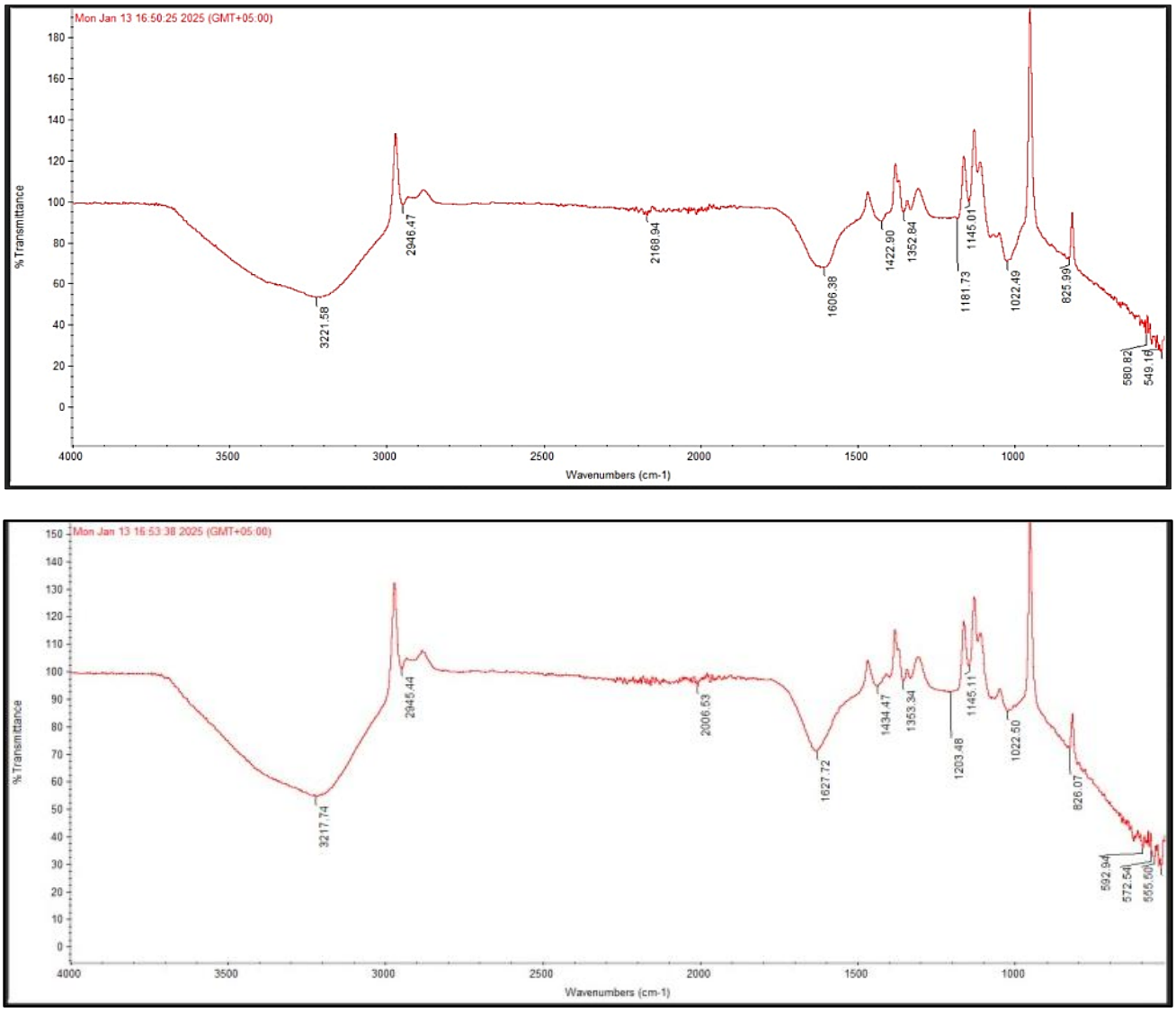

Fig. 3. FTIR analysis graph (a) with and (b) without Bacillus subtilis.

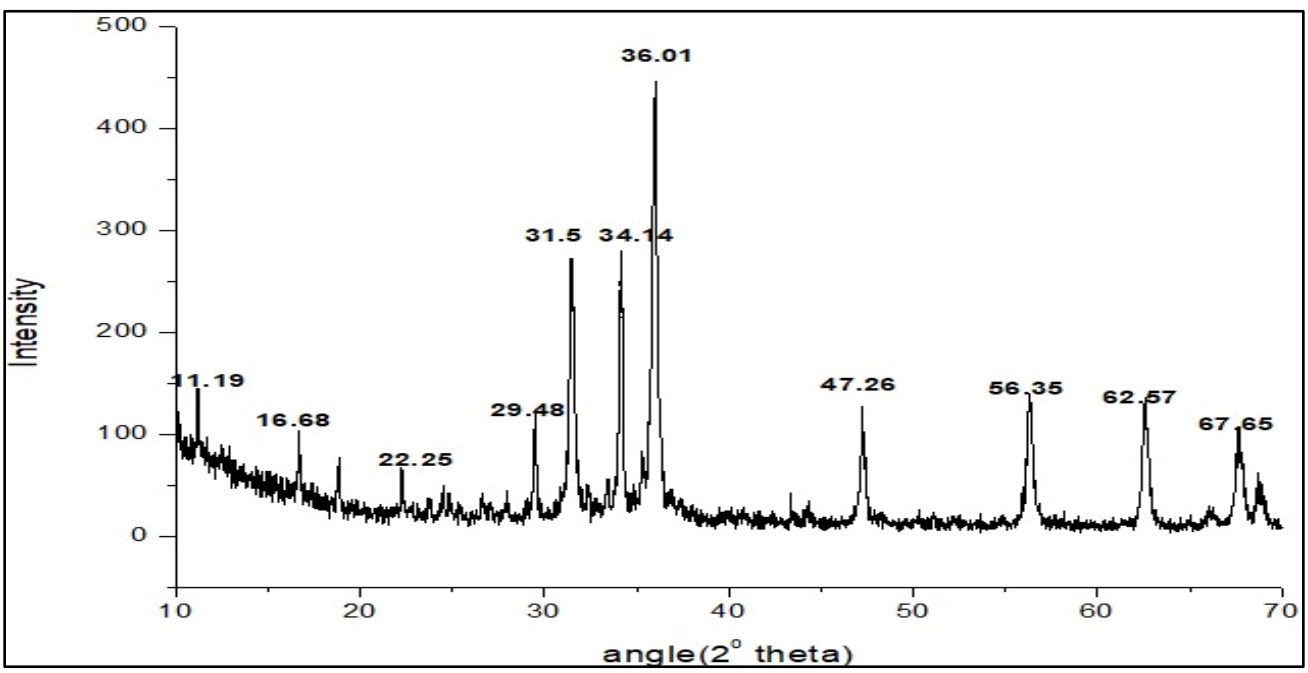

Fig. 1. XRD pattern of synthesized starch beads or capsule.

Table 2 Antifungal activities of the starch with and without *Bacillus subtilis*

Pathogen	Starch nanobeads with *Bacillus subtilis*		Standard antifungal drug (Nystatin)	
	Disc diffusion or Inhibition zone (mm) with S.D (X ±S.D)	Minimal fungicidal concentration (MFC) (mg mL−1)	Disc diffusion or Inhibition zone (mm) with S.D (X ±S.D)	Minimal inhibitory concentration (MIC) (ug mL−1)
Fusarium oxysporum	39.03 ± 0.34	0.7	20. 11 ± 0.41	50
Fusarium graminearum	29.51 ± 0.9	1.00	15.02 ± 0.02	32
Fusarium culmorum	52.47 ± 0.03	0.53	29.32 ± 0.72	64
Aspergillus flavus	22.36 ± 0.81	0.52	11.23 ± 0.04	71
Alternaria solani	30.31 ± 0.02	0.40	14.81 ± 0.76	128
Botrytis cinerea	41.12 ± 0.21	0.61	19.72 ± 0.91	nil
Verticillium dahliae	24.25 ±0.92	0.43	15.11 ± 0.24	130
Cladosporium cucumerinum	21.41 ± 0.52	0.32	14.22 ± 0.71	128

Antifungal activity: Antifungal activity of starch beads or capsules containing *Bacillus subtilis* against *Fusarium oxysporum, Fusarium graminearum, Aspergillus flavus, Alternaria solani, Botrytis cinerea, Verticllium dahlia,* and *cladosporium cucumirinum* was analyzed using a disc diffusion method. A clear inhibition zone was observed that indicates the significant antifungal effect of the sample. Table 2 indicates an inhibition zone of different diameters.

Antifungal activity of nanobeads with and without *Bacillus subtilis* was tested on different types of fungus pathogens through disc diffusion method. Starch nanoparticles are potential antibacterial agents and their efficiency enhanced through the encapsulation of *Bacillus subtilis*, similarly the present work revealed the higher antifungal activities of starch nanoparticles encapsulated with *Bacillus subtilis* than starch nanoparticles without *Bacillus subtilis* as indicated by MIC and DD. The MIC of starch nanobeads encapsulated with *Bacillus subtilis* was 0.7 mg mL−1 for *Fusarium oxysporum,* 1 mg mL−1 for *Fusarium graminearum,* 0.5 mg mL−1 *for Fusarium culmorum,* 0.5 mg mL−1 for *Aspergillus flavus*, 0.4 mg mL−1 for *Alternaria solani,* 0.5 mg mL−1 for *Botrytis cinerea,* 0.4 mg mL−1 for *Verticillium dahlia*, and 0.4 mg mL−1 for *Cladosporium cucumerinum* (Table 2). The primary well diffusion assay revealed significant antifungal activity of starch nanobeads encapsulated with *Bacillus subtilis* against all the tested fungus pathogens. In general, plant-associated bacteria are more likely to compete with soil-borne diseases, such *Fusarium*, that infect plants through mycelia contact (Fira *et al*., 2018). Bacon *et al*., claimed that because *Bacillus subtilis* and *Fusarium* spp., share an ecological niche based on competitive exclusion, *Bacillus subtilis* may be able to prevent *Fusarium* spp., infection in maize plants. Proteases and chitinases are examples of lytic enzymes that exhibit direct antifungal effects by breaking down fungal cell walls and preventing fungal growth *In vitro* (Ramyabharathi & Raguchander, 2014). from a theoretical standpoint agriculture utilizes biofertilizers to enhance plant growth and encapsulated nano fungicides in animal feed to enhance health and growth (Sowmeya & Sathiavelu, 2024). However, the antifungal activity might be varied based on the interaction of bacterial enzyme with starch nanoparticles. Therefore, this work opens the new door for further study to find out the interaction between encapsulated nanoparticles and different pathogens.

Conclusion

The present study successfully enhanced the antifungal activity of *Bacillus subtilis* by encapsulating it in starch. *Bacillus subtilis* molecules were used as a capping agent to effectively produce nanoparticles (NPs) both with and without encapsulation, as confirmed by FTIR analysis. X-ray diffraction (XRD) analysis exhibited distinct crystalline peaks at 11.19◦, 16.68◦, 22.25◦, 29.48◦, 36.01◦, 47.26◦, 56.35◦, 62.57◦, and 67.65◦ in the *Bacillus subtilis*-loaded microbeads, ensuring the *Bacillus subtilis* and starch interactions for stable crystalline structure formation. XRD and SEM analyses revealed the polydisperse, spherical, and crystalline nature of both encapsulated starch nanoparticles. These findings were further supported by Fourier transform infrared (FTIR) spectroscopy by depicting characteristic peaks like 3221.58 cm− 1 (N–H stretching), 2946.47 cm− 1 (C–H stretching), and 1606.38 cm− 1 (C– –C stretching), ensuring the probiotic presence by functional groups within the starch matrix. These FTIR and XRD analyses provide detailed insight into the molecular interactions between *Bacillus subtilis* and starch. Additionally, the presence of a coating around the nanoparticles confirmed the successful starch encapsulation. Zeta potential analysis indicated significant differences in nanoparticle sizes, with the encapsulated particles being larger than those without encapsulation, as observed by SEM. Furthermore, the cell toxicity test results demonstrated that starch encapsulation reduced the toxicity of the cells. Overall, this study highlights the effectiveness of starch encapsulation in enhancing the antimicrobial activity of NPs against fungal pathogens. To further improve nanoscale interactions between *Bacillus subtilis* and starch, future research should focus on refining the encapsulation process and exploring additional characterization methods.

Acknowledgement

This data is part of the Ph.D. thesis research conducted by Ms. Ayesha Khan

Author's contribution: Ayesha Khan**:** Methodology, Software, Formal Analysis, Writing original draft, review and editing, Sadia Javed**:** Conceptualization, Resources, Project Administration, Validation, Supervision, Writing, review and editing

Confilict of interest: There is no conflict of interest.

References

Adamson, D. and S. Bray. 1999. The economic benefit from investing in insect biological control of parthenium weed *(Parthenium hysterophorus)*. Department of Natural Resources.

Ahmad, M. and A. Gani. 2021. "Development of novel functional snacks containing nano-encapsulated resveratrol with anti-diabetic, anti-obesity and antioxidant properties." *Food Chemistry*, **352**: 129323.

Ahmad, S., S. Munir, N. Zeb, A. Ullah, B. Khan, J. Ali and S. Ali. 2019. Green nanotechnology: A review on green synthesis of silver nanoparticles—An ecofriendly approach. *International Journal of Nanomedicine*, 5087-5107.

Alhaithloul, H.A., N.S. Awad, T. Shoala, M.M. Alqahtani, F.M. Alzuaibr, A. Alasmari and M.A. Abdein. 2024. Comparison of various hormone combinations and the potential of chitosan nanoparticles for growth stimulation in *Astragalus* spp. *Plant Cell, Tissue and Organ Culture (PCTOC)*, 157(3): 74.

Afzaal, H., A.A. Farooque, F. Abbas, B. Acharya and T. Esau. 2020. Precision irrigation strategies for sustainable water budgeting of potato crop in Prince Edward Island. *Sustainability*, 12(6): 2419.

Akalin, G.O. and M. Pulat. 2020. Controlled release behavior of zinc-loaded carboxymethyl cellulose and carrageenan hydrogels and their effects on wheatgrass growth. *Journal of Polymer Research*, 27(1): 6.

Atraki, R. and M. Azizkhani. 2021. "Survival of probiotic bacteria nanoencapsulated within biopolymers in a simulated gastrointestinal model." *Innovative Food Science & Emerging Technologies*, **72**: 102750.

Ashwar, B.A., A. Shah, A. Gani, S.A. Rather, S.M. Wani, I.A. Wani and A. Gani. 2014. Effect of gamma irradiation on the physicochemical properties of alkali-extracted rice starch. *Radiation Physics and Chemistry*, 99: 37-44.

Azeem, M., M.Z. Haider, S. Javed, M.H. Saleem and A. Alatawi. 2022. Drought stress amelioration in maize (*Zea mays* L.) by inoculation of *Bacillus* spp., strains under sterile soil conditions. *Agriculture*, 12(1): 50.

Bashir, S., S. Javed, K.M. Al-Anazi, M.A. Farah and S. Ali. 2022. Bioremediation of cadmium toxicity in wheat (*Triticum aestivum* L.) plants primed with L-Proline, *Bacillus subtilis* and *Aspergillus niger. Inter. J. Environ. Res. and Public Health*, 19(19): 12683.

Barton, L.M., E.J. Duval, E. Stroberg, S. Ghosh and S. Mukhopadhyay. 2020. Covid-19 autopsies, oklahoma, usa. *Amer. J. Clin. Pathol*., 153(6): 725-733.

Brindha, B., M.K. Okla, S. Kokilavani, L. Sabariselvan, S.S. Al-amri, M.A. Abdel-Maksoud and S. Khan. 2024. Dynamic Ag-mediated electron transfer confined ZnO nanorods for boosted photocatalytic bacterial disinfection. *Journal of Cleaner Production*, 451: 141908.

Chauhan, A. and P. Chauhan. 2014. Powder XRD technique and its applications in science and technology. *J. Anal. Bioanal Tech*., 5(5): 1-5.

Cruz-Luna, A.R., H. Cruz-Martínez, A. Vásquez-López and D.I. Medina. 2021. Metal nanoparticles as novel antifungal agents for sustainable agriculture: Current advances and future directions. *Journal of Fungi*, 7(12): 1033.

Dong, X., J. Bao, D. Chen, W. Zhang, N. Yu, L. Yuan and B. Guo. 2022. Cswin transformer: A general vision transformer backbone with cross-shaped windows. In *Proceedings of the IEEE/CVF Conference on Computer Vision and Pattern Recognition*, pp. 12124-12134.

Elnahal, A.S., M.T. El-Saadony, A.M. Saad, E.S.M. Desoky, A.M. El-Tahan, M.M. Rady and K.A. El-Tarabily. 2022. The use of microbial inoculants for biological control, plant growth promotion, and sustainable agriculture: A review. *European Journal of Plant Pathology*, 162(4): 759-792.

Feng, S., D.J. Phillips, T. White, H. Sayal, P.K. Aley, S. Bibi and M. Voysey. 2021. Correlates of protection against symptomatic and asymptomatic SARS-CoV-2 infection. *Nature Medicine*, 27(11): 2032-2040.

Fira, D., I. Dimkić, T. Berić, J. Lozo and S. Stanković. 2018. Biological control of plant pathogens by *Bacillus* species. *Journal of Biotechnology*, 285: 44-55.

Fareez, I.M., S.M. Lim, R.K. Mishra and K. Ramasamy. 2015. Chitosan coated alginate–xanthan gum bead enhanced pH and thermotolerance of *Lactobacillus plantarum* LAB12. *International Journal of Biological Macromolecules*, 72: 1419-1428.

Gul, S., S. Javed, M. Azeem, A. Aftab, N. Anwaar, T. Mehmood and B. Zeshan. 2023. Application of *Bacillus subtilis* for the alleviation of salinity stress in different cultivars of wheat (*Tritium aestivum* L.). *Agronomy*, 13(2): 437.

Gopalakrishnan, V., C.N. Spencer, L. Nezi, A. Reuben, M.C. Andrews, T.V. Karpinets and J. Wargo. 2018. Gut microbiome modulates response to anti–PD-1 immunotherapy in melanoma patients. *Science*, 359(6371): 97-103.

Hassainia, A., H. Satha and S. Boufi. 2018. Chitin from Agaricus bisporus: Extraction and characterization. *Inter. J. Biol. Macromol.*, 117: 1334-1342.

Javed, S., A. Ali, S. Alam, M. Rafique, B. Gul, H.J. Chaudhary and E.Y. Santali. 2024. Biosorption of cadmium and chromium from wastewater using *Bacillus xiamenensis* and *Bacillus cereus* isolated from the sugarcane rhizosphere. *ACS ES & T Water*, 4(9): 4140-4149.

John, K., A. Knyazeva and D. Knyazeva. 2011. Does geography matter? Firm location and corporate payout policy. *J. Financial Econ.*, 101(3): 533-551.

Jurat-Fuentes, J.L., D.G. Heckel and J. Ferré. 2021. Mechanisms of resistance to insecticidal proteins from *Bacillus thuringiensis. Annu. Rev. Entomol*., 66(1): 121-140.

Kleindorfer, D.O., A. Towfighi, S. Chaturvedi, K.M. Cockroft, J. Gutierrez, D. Lombardi-Hill and L.S. Williams. 2021. Guideline For the prevention of stroke in patients with stroke and transient ischemic attack: A guideline from the American Heart Association/American Stroke Association. *Stroke*.

Le Quéré, C., R.M. Andrew, J.G. Canadell, S. Sitch, J.I. Korsbakken, G.P. Peters and S. Zaehle. 2016. Global carbon budget 2016. *Earth System Science Data*, 8(2): 605-649.

Martin, F.J., M.R. Amode, A. Aneja, O. Austine-Orimoloye, A.G. Azov, I. Barnes and P. Flicek. 2023. Ensembl 2023. *Nucleic Acids Res.*, 51(D1): D933-D941.

McMullan, G., K. Naydenova, D. Mihaylov, K. Yamashita, M.J. Peet, H. Wilson and C.J. Russo. 2023. Structure determination by cryoEM at 100 keV. *Proceedings of the National Academy of Sciences*, 120(49): e2312905120.

Murhekar, M.V., T. Bhatnagar, J.W.V. Thangaraj, V. Saravanakumar, M.S. Kumar, S. Selvaraju and A. Vinod. 2021. SARS-CoV-2 seroprevalence among the general population and healthcare workers in India, December 2020–January 2021. *Inter. J. Infectious Dis.*, 108: 145-155.

Masoudipour, E., H. Amirian and R. Sahraeian. 2017. A novel closed-loop supply chain based on the quality of returned products. *Journal of Cleaner Production*, 151: 344-355.

Noman, M., T. Ahmed, J. Wang, M. Ijaz, M. Shahid, M.S. Islam and F. Song. 2023. Nano-enabled crop resilience against pathogens: Potential, mechanisms and strategies. *Crop Health*, 1(1): 15.

Nichols, E., J.D. Steinmetz, S.E. Vollset, K. Fukutaki, J. Chalek, F. Abd-Allah and X. Liu. 2022. Estimation of the global prevalence of dementia in 2019 and forecasted prevalence in 2050: an analysis for the Global Burden of Disease Study 2019. *The Lancet Public Health*, 7(2): e105-e125.

Olatunde, S. 2024. Quantum Mechanical Evaluation and Molecular Modeling of SARS-CoV-2 Main Drivers: A Computational Study on Putative Inhibitors for Drug Discovery.

Paredes, M.F., D. James, S. Gil-Perotin, H. Kim, J.A. Cotter, C. Ng and A. Alvarez-Buylla. 2016. Extensive migration of young neurons into the infant human frontal lobe. *Science*, 354(6308): aaf7073.

Ramyabharathi, S.A. and T. Raguchander. 2014. Mode of action of *Bacillus subtilis* EPCO16 against tomato *Fusarium wilt. Biochem. Cell. Arch*., 14(1): 47-50.

Remanan, M.K. and F. Zhu. 2021. Encapsulation of rutin using quinoa and maize starch nanoparticles. *Food Chemistry*, 353: 128534.

Robson, J.C., P.C. Grayson, C. Ponte, R. Suppiah, A. Craven, A. Judge and K. Liang. 2022. 2022 American College of Rheumatology/European Alliance of Associations for Rheumatology classification criteria for granulomatosis with polyangiitis. *Arthritis & Rheumatology*, 74(3): 393-399.

Sandhya, M., D. Ramasamy, K. Sudhakar, K. Kadirgama and W.S.W. Harun. 2021. Ultrasonication an intensifying tool for preparation of stable nanofluids and study the time influence on distinct properties of graphene nanofluids–A systematic overview. *Ultrasonics Sonochemistry*, 73: 105479.

Santoso, A., R. Pranata, A. Wibowo, M.J. Al-Farabi, I. Huang and B. Antariksa. 2021. Cardiac injury is associated with mortality and critically ill pneumonia in COVID-19: a meta-analysis. *The Amer. J. Emer. Med*., 44: 352-357.

Shahzad, Q., S. Mahmood, S. Javed and T. Mushtaq. 2021 Chromium stress tolerance of a C4 (*Zea mays* L.) and C3 (*Vigna radiata* L.) plants primed with UV and Gamma-treated *Bacillus subtilis*. *Microorganisms*, 9(11): 2313.

Shoukat, L., S. Javed, M. Afzaal, N. Akhter and Y.A. Shah. 2024. Starch-based encapsulation to enhance probiotic viability in simulated digestion conditions. *Inter. J. Biol. Macromol.*, 283: 137606.

Sowmeya, V.G. and M. Sathiavelu. 2024. Development of microbial biotechnology products for sustainable agriculture. In *The Potential of Microbes for a Circular Economy* pp. 219-252. Academic Press.

Sun, J., X. Li, J. Feng and X. Tian. 2009. Oxone/Co2+ oxidation as an advanced oxidation process: Comparison with traditional Fenton oxidation for treatment of landfill leachate. *Water Research*, 43(17): 4363-4369.

Yadav, M., T. Kumar, A. Kanakan, R. Maurya, R. Pandey and N.S. Chauhan. 2022. Isolation and characterization of human intestinal bacteria *Cytobacillus oceanisediminis* NB2 for probiotic potential. *Frontiers in Microbiology*, 13: 932795.

Zubair, T. and D. Bandyopadhyay. 2023. Small molecule EGFR inhibitors as anti-cancer agents: Discovery, mechanisms of action, and opportunities. *Inter. J. Mol. Sci.*, 24(3): 2651.